Modeling of Parasitic Hydrogen Evolution Effects in an Aluminum-air Cell

Huizhi Wang, [†] *Dennis Y.C. Leung,* [*,†] *Michael K.H. Leung,* [†] *and Meng Ni* [‡]

[†]Department of Mechanical Engineering, The University of Hong Kong, Pokfulam Road, Hong Kong, China

[‡]Department of Building and Real Estate, Hong Kong Polytechnic University, Hung Hom, Kowloon, Hong Kong, China

ABSTRACT The aluminum-air battery has potential to serve as a near-term power source for electric vehicles. Parasitic hydrogen evolution caused by anode corrosion during the discharge process, however, has long been recognized as an obstacle to further commercialization of the aluminum-air battery. This paper focuses on the parasitic reaction impacts with an aim of better understanding and managing the parasitic reaction. On the basis of a mathematical model, effects of the parasitic hydrogen evolution on cell flow field, ionic mass transfer and current density are investigated. Besides, the possibility of utilizing the parasitically evolved hydrogen to increase the total power output is evaluated.

KEYWORDS: Aluminum air cell; hydrogen evolution; computational fluid dynamics (CFD); numerical simulation

[*] To whom correspondence should be addressed. Tel: +852 2859 7911; Fax: +852 2858 5415. E-mail address: ycleung@hku.hk(Dennis Y.C. Leung).

Introduction

The aluminum-air battery, owning a theoretical open-circuit voltage of 2.73V and specific energy (8.1kWh/(kg of Al); 2.8kWh/(kg of cell reactants)) second only to lithium-air battery, has potential to serve as a near-term power source for electric vehicles. Other advantages of the aluminum-air battery include its economical cost, low environmental impact as well as safety. Parasitic hydrogen evolution caused by anode corrosion during the discharge process has long been recognized as an obstacle to further commercialization of the aluminum-air battery as it not only causes additional consumption of the anode material but also increases the ohmic loss in the cell. Efforts to suppress the parasitic corrosion include doping high purity grade aluminum (99.999% grade)[1] with particular alloying elements[2] and introducing corrosion inhibitors into electrolyte[3]. Nevertheless, doing these will definitely increase the cell production costs. Recently, Zhuk et al.[4] experimentally studied the feasibility of the utilization of the parasitically produced hydrogen and proposed a conceptual electricity-hydrogen cogenerating system using low grade aluminum. To better understand and manage the parasitic reaction, this paper therefore aims to give an in-depth investigation of the parasitic reaction effects based on a mathematical model. Influences of the parasitic hydrogen evolution on the cell flow field, ionic mass transfer and current density are simulated. Possible contributions from the evolved hydrogen to the total power output are also estimated.

Mathematical Model

Problem Description. Simulations in this study are carried out with an aluminum-air cell depicted in Figure 1. The cell consists of two parallel plane electrodes with cell gap (S) and height (L). Pure aluminum (99.99% grade) is used as the anode material and 5% cobalt tetamethoxyphenyl porphyrin (CoTMPP) on steam-activated Sawinigan acetylene black[5] is used for the air diffusion cathode. 5M KOH electrolytic solution enters the cell from the inlet at the bottom. To avoid the boundary impacts, both

inlet and outlet are set to be sufficiently far from the electrode region, denoted as *L'* in the figure. The following set of half-cell reactions is considered:

1. main reaction at the anode and cathode:

$$Al + 4OH^- \rightarrow Al(OH)_4^- + 3e^- \tag{1}$$

$$O_2 + 2H_2O + 4e^- \rightarrow 4OH^- \tag{2}$$

2. parasitic reaction at the anode [6]

$$Al + 3H_2O + OH^- \rightarrow \frac{3}{2}H_2 + Al(OH)_4^- \tag{3}$$

General assumptions applied to this modeling work include: i) Laminar, incompressible flow; ii) Constant transference numbers equal to their bulk values; iii) Hydrogen bubbles are spherical with an identical diameter; iv) Surface shadowing is neglected; v) The cathode is treated as a planar electrode with a simplified linear kinetic expression; vi) No crystallization reaction occurs; vii) Isothermal conditions exists; and viii) Steady-state condition exists. Assumptions i)-vi) have already been adopted and justified elsewhere[6-12] and the last two assumptions could be easily modified to account for thermal effects as well as dynamic behaviors. The modeling details are described in the following subsections.

Governing Equations. On the basis of the above-stated assumptions, modeling equations are developed for the conservations of mass, momentum, charge and ionic species.

Mass and momentum conservations. - The continuity and momentum equations for the mixture of the liquid electrolyte and parasitically produced gas respectively are

$$\frac{\partial(\rho_{mix})}{\partial t} + \nabla(\rho_{mix} v_{mix}) = 0 \tag{4}$$

$$\frac{\partial(\rho_{mix} v_{mix})}{\partial t} + \nabla(\rho_{mix} v_{mix} v_{mix}) = -\nabla p + \rho_{mix} g + \nabla \overline{\overline{\tau}}_{mix} - \nabla\left[\left(1 - \frac{f_g \rho_g}{\rho_{mix}}\right) f_g \rho_g v_{\lg} v_{\lg}\right] \tag{5}$$

where subscripts *l*, *g* and *mix* refer to liquid, gas and mixture, f denotes the phasic volume fraction, $\overline{\overline{\tau}}$ denotes the stress-strain tensor (N/(m^{3}s)), the mixture density $\rho_{mix} = f_l\rho_l + f_g\rho_g$ (kg/m^3), the mass-averaged mixture velocity $v_{mix} = \left(f_l\rho_l v_l + f_g\rho_g v_g\right)/\rho_{mix}$ (m/s), the relative velocity between the gas and liquid phase, v_{lg} (m/s), is formulated to be[13]

$$v_{\mathrm{lg}} = \left[\frac{4d_g^2\left(\rho_g - \rho_{mix}\right)}{3C_D\,\mathrm{Re}\,\mu_l}\right]\left[g - \frac{\partial v_{mix}}{\partial t} - \left(v_{mix}\cdot\nabla\right)v_{mix}\right] \tag{6}$$

In the above, d_g denotes the bubble diameter (m), μ_l denotes the electrolyte viscosity (kg/(ms)), Re denotes the relative Reynolds number ($\mathrm{Re} = \frac{\rho_l\left|v_g - v_l\right|d_g}{\mu_l}$), and the drag coefficient, C_D, is determined from the Morsi and Alexander drag model[10]: $C_D = k_1 + k_2/\mathrm{Re} + k_3/\mathrm{Re}^2$ ($k_{1\sim3}$ are semi-empirical constants obtained with rigid spherical particles).

The transport equation for the gas volume fraction is derived by re-arranging the continuity equation of the gas phase:

$$\frac{\partial\left(f_g\rho_g\right)}{\partial t} + \nabla\left(f_g\rho_g v_{mix}\right) = -\nabla\left[f_g\rho_g\left(1 - \frac{f_g\rho_g}{\rho_{mix}}\right)v_{\mathrm{lg}}\right] + S_g \tag{7}$$

where S_g corresponds to the mass production rate of hydrogen from the parasitic reaction at the anode (kg/(m^{3}s)) and is estimated using Faraday's law as

$$S_g = \frac{M_{H_2}A_a\left|J_p\right|}{2F} \tag{8}$$

In the above, M_{H2} is the molar mass of hydrogen (~0.002 kg/mol), A_a is the electroactive interfacial area per unit volume of anode (1/m), J_p is the transfer current density resulting from the parasitic reaction described in the following subsection (A/m^2), and F is the Faraday's constant.

With a solved gas volume fraction, the volume fraction of electrolyte can be calculated according to the following relationship held in the flow field:

$$f_l = 1 - f_g \tag{9}$$

Charge conservation. - As generalized by Wang[14], conservation principles for charge and species can be written in a convection-diffusion-source form. The potential field in the electrolyte is consequently described as

$$\nabla(-\kappa^{eff}\nabla\phi) = AJ + F\sum_j z_j \nabla\left(D_j^{eff}\nabla C_j\right) \tag{10}$$

where C is the species concentration (mol/m^3), z is the charge number, A is the electroactive interfacial area per unit volume of electrodes (A=A_a at the anode, and A=A_c at the cathode) (1/m), κ^{eff} and D^{eff} respectively are the effective conductivity (S/m) and species diffusivity (m^2/s) in the mixture, which have been correlated to their gas free values (κ_0, D_0) through the Bruggeman formula[15]

$$\kappa^{eff} = \kappa_0\left(1-f_g\right)^{1.5};\ D_i^{eff} = D_{i,0}\left(1-f_g\right)^{1.5} \tag{11}$$

The first source term at the right-hand side of Eq. (10) represents the volumetric transfer current density resulting from the electrochemical reaction at the electrode/electrolyte interface. Thus, it is zero in most of the computational zone and non-zero only in the control volumes adjacent to the electrode/electrolyte interface. The second source term of Eq. (10) represents the diffusion current effects raised by the species concentration gradients.

Kinetics of the electrochemical reactions at the anode are described as[11]

$$J_m = J_{m0}\left[\left(\frac{C_{OH^-}^{SA}}{C_{OH^-}^{ref}}\right)^{\gamma_m}\exp\left(\frac{\alpha_m n_m \eta_m F}{RT}\right) - \left(\frac{C_{Al(OH)_4^-}^{SA}}{C_{Al(OH)_4^-}^{ref}}\right)^{\lambda_m}\exp\left(\frac{-\beta_m n_m \eta_m F}{RT}\right)\right] \tag{12}$$

$$J_p = J_{p0}\left[-\exp\left(\frac{-\beta_p n_p \eta_p F}{RT}\right)\right] \tag{13}$$

where subscripts m and p respectively denote main and parasitic reaction, η denotes the overpotential (V), $C_{OH^-}^{ref}$ and $C_{Al(OH)_4^-}^{ref}$ are the inlet concentrations (mol/m^3) and serve as the reference concentrations, $C_{OH^-}^{SA}$ and $C_{Al(OH)_4^-}^{SA}$ are the surface concentrations at the anode (mol/m^3), J_0 is the exchange current density defined at the reference concentrations (A/m^2), R is the ideal gas constant (equal to 8.314J/(mol K)), T is the operating temperature (K), γ and λ are the coefficients that depend on the mechanism and stoichiometry of the reaction, α is the anodic transfer coefficient for the reaction, β is the cathodic transfer coefficient for the reaction, and n is the number of electrons transferred in the rate-limiting step of the reaction.

The cathode kinetics is simplified using a linear correlation[12]

$$J_c = k\eta_c + b \tag{14}$$

where k and b are constants related to the electrode properties.

Surface overpotentials that drive different electrochemical reactions are defined as follows

$$\eta_m = E_c^{eq} - E_m^{eq} - V_{cell} - \phi\,;\ \eta_p = E_c^{eq} - E_p^{eq} - V_{cell} - \phi\,;\ \eta_c = -\phi \tag{15}$$

where E^{eq} represents the equilibrium potential (V) with respect to a common reference electrode and at the reference concentrations used for the kinetic expressions, and V_{cell} represents the cell voltage (V) prescribed for each computation.

Species conservation. - The conservation of dissolved ionic species in the two-phase medium is accordingly given by inserting a modified Nernst-Planck equation into the general material balance equation

$$\begin{aligned}&\frac{\partial[(1-f_g)C_i]}{\partial t} + \nabla\left[v_l(1-f_g)C_i - D_{i,0}(1-f_g)^{1.5}\nabla C_i\right] \\ &= -\frac{t_i}{z_i}\sum_j z_j \nabla\left[D_{j,0}(1-f_g)^{1.5}\nabla C_j\right] - \frac{t_i}{z_i F}AJ + S_i\end{aligned} \tag{16}$$

where t is the ion transference number. The volumetric source term S_i (mol/(m^{3}s)) in the above accounts for the ion production or consumption resulting from the electrochemical reactions at the electrode/electrolyte interface. Therefore, S_i is also confined in a layer of control volumes neighboring the electrode/electrolyte interface and zero in other computational zone.

According to Eqs. 1-3, three ionic species, $Al(OH)_4^-$, OH^- and K^+, need to be considered in the aluminum-air cell. In this paper, only concentrations of $Al(OH)_4^-$ and OH^- are solved from Eq. 16 while the concentration of K^+ is determined from the known concentrations of $Al(OH)_4^-$ and OH^- with the electroneutrality condition($\sum_j z_j C_j = 0$). Corresponding S_i terms for OH^- and $Al(OH)_4^-$ are evaluated from Faraday's law and in the form of

$$S_{OH^-} = \begin{cases} -\dfrac{4A_a J_m}{3F} + \dfrac{A_a J_p}{3F} & \text{at the anode} \\ -\dfrac{A_c J_c}{F} & \text{at the cathode} \end{cases} \tag{17}$$

$$S_{Al(OH)_4^-} = \begin{cases} \dfrac{A_a J_m}{3F} - \dfrac{A_a J_p}{3F} & \text{at the anode} \\ 0 & \text{at the cathode} \end{cases} \tag{18}$$

Under the steady state, the first term at the left-hand side of Eq. 16 vanishes.

In general, Eqs.4, 5, 7, 9, 10 and 16 constitute a complete governing equation system for (i+5) unknowns: v, p, f_g, f_l, ϕ, and C_i. Their corresponding boundary conditions are

Hydrodynamics:

$$v_l = v_0 ,\ f_g = 0 \text{ at the inlet; } p = p_{out} \text{ at the outlet} \tag{19}$$

Concentrations:

$$C_i = C_i^{ref} \text{ at the inlet; } \frac{\partial C_i}{\partial \vec{n}} = 0 \text{ at other boundaries} \tag{20}$$

Potential:

$$\frac{\partial \phi}{\partial n} = 0 \text{ at all boundaries} \tag{21}$$

It should be noted that non-flux boundaries are specified to the electrodes here for both concentrations and potential because any production or consumption of species and charge has been included as a source term appearing in the governing equations.

Numerical Procedures. Since all governing equations have been intentionally written in a convective-diffusion-source form[14], they are able to be discretized by finite-volume method and solved using the commercial CFD code, FLUENT 6.2. Charge and species conservations are solved as User-Defined Scalars implemented with a set of User-Defined Functions written in C language dynamically linked to the FLUENT source code. In the following sections, two sets of geometrical parameters as tabulated in Table I are used for simulations. The cell 1, corresponding to the AT400 design of aluminum cell built by Eltech Systems Corporation, Chardin, Ohio[11], is adopted for the model validation. Further analysis is based on the simulations on the cell 2 in order to save computation time. Non-uniform 18×929 and 28×654 grid schemes in the *x*, *y* directions with mesh refinement near the electrodes are respectively selected for cell 1 and cell 2 after a grid independence check.

Results and Discussion

Model Validation. To evaluate the validity of the present model, comparisons were made to the reported experimental data for an AT400 cell operated at a temperature range of 331~333K with inlet electrolyte velocity of 0.017m/s[11]. Input parameters to simulations correspond to the experimental conditions and are listed in Table I. Figure 2 shows the predicted *J-V* characteristic curve compared with the measured data. A good agreement with the maximum deviation of 12.23% of the measured results can be observed in this figure and thus validates our numerical model.

Hydrogen and Velocity Distributions. Figure 3 illustrates the predicted hydrogen distribution at an operating cell voltage of 1.3V. Figure 3(a) corresponds to the whole cell plus entrance region and Figure

3(b) focuses on the cell gap between two electrodes. Less than quarter of the cell gap is displayed on the x axis for both figures in order to give a clearer view. In the x direction, hydrogen volume fraction is observed to achieve its largest value at the gas-evolving anode (x=0) and then decrease sharply within a thin layer adjacent to the anode while the bulk flow can still be regarded as single phase. In the y direction, an increasing volume fraction with height is found, attributed to the accumulation of gas released at lower part of the cell. Corresponding mixture velocity distributions are shown in Figure 4. It is worth mentioning that a low inlet velocity (i.e. v_0=0.017m/s) is chosen for study here aiming to magnify the bubble impact. An enhanced convective flow caused by the buoyant gas stream can be seen near the anode, which distorts the fully developed parabolic velocity profile at the cell entrance.

Hydrogen Evolution Effects on Ionic Mass Transfer. Distributions of OH^- and $Al(OH)_4^-$, the two electroactive ions involved in the cell reactions, are depicted in Figure 5. Figure 5(a) and 5(c) are modeled with single-phase condition in which we assume an ideal alloy with kinetics of negligible J_{p0} (i.e. no parasitic corrosion), while Figure 5(b) and 5(d) correspond to the practical two-phase condition. Through a comparison, at the anode, an enhanced mass transfer corresponding to a thinner concentration boundary layer is found with the gas evolution, which is mainly due to i) a bubble-induced convection as described in the foregoing subsection; and ii) reduction in species diffusivity according to the Bruggemann correlation (Eq.11). The bubble-induced enhancement of OH^- transfer at the anode can effectively prevent the OH^- depletion and thus mass transfer limited cell performance. Ionic mass transfer at the cathode, however, is significantly inhibited by the presence of bubbles as the velocity is reduced near the cathode. Although mass transfer alteration at the cathode seems not to affect the cell performance according to the kinetic expressions adopted in this study, this process might be of importance for situations in which the non gas-evolving electrode kinetics is mass transfer determined.

Hydrogen Evolution Effects on Current Density Distribution. The parasitically evolved hydrogen affects the current density distribution in the cell mainly through two aspects: first, bubbles enhance the OH^- mass transfer at the anode and therefore lead to a more uniform current distribution along the

electrodes; second, bubbles alter the electrolyte conductivity and increase the ohmic resistance. The first aspect has been discussed in the above subsection, and the variation of electrical conductivity averaged over the cell gap (*x* direction) along the *y* direction is plotted in Figure 6. The averaged conductivity gradually decreases along *y* axis due to the accumulation of produced hydrogen. Resulting current density distributions in the *y* direction at different electrolyte inlet velocities compared with those calculated under the single-phase condition are shown in Figure 7. At both low (i.e. v_0=0.017m/s) and high (i.e. v_0=0.08m/s) inlet velocities, current densities predicted with bubbles are slightly lower than those predicted without bubbles because of an increased ohmic loss. The higher inlet velocity corresponds to higher current densities since electrolyte flow with high speed helps to homogenize the OH^- distribution for the single-phase cases and facilitates the removal of bubbles for the two-phase cases.

Hydrogen Contribution Evaluation. Power output from the evolved hydrogen is roughly estimated by $\eta_{eff}\Delta_R G_T^0 \frac{J_p}{2F}$, where η_{eff} is the utilization efficiency of hydrogen and $\Delta_R G_T^0$ is the standard Gibbs energy of water formation and equal to -237kJ/mol. To better quantify the extent to which aluminum energy is used, the aluminum utilization efficiency, defined as the ratio of generated specific energy to the theoretical one of aluminum (8.1kWh/kg), is analyzed as shown in Figure 8. The aluminum utilization efficiency with the parasitic reaction is much lower than that of the ideal anode alloy with no parasitic reaction, especially at large operating voltages if only the electric power produced by the aluminum-air cell is taken into account, because large cell voltages correspond to small current densities and thus large parasitic current densities. Supposing that the parasitically evolved hydrogen is further delivered to a fuel cell with an efficiency of 50%, the aluminum utilization efficiency with parasitic reaction can be raised to approach 46.5% at the cell voltage of 1.6V but still lower than that in the absence of parasitic reaction. Aluminum utilization efficiencies in both cases of practical anode and ideal anode in a wide range of cell voltages can be comparable provided that all produced hydrogen is fully utilized.

Conclusions

A model coupling together electrochemical kinetics, species transport and two-phase hydrodynamics has been developed to describe the parasitic hydrogen evolution during the discharge of aluminum-air cell. Comparisons between the simulation results and experimental data show a good agreement. Hydrogen distribution in the cell was visualized and found to significantly affect the cell flow field as a buoyancy-induced convective flow occurs, especially at the vicinity of the gas-evolving anode where bubble volume fraction is large. Comparing to the calculation results from a model excluding parasitic reaction, hydrogen was found to lead to a more uniform distribution of ions at the anode but retard the ionic mass transfer at the cathode partially due to the alteration of velocity field and partially the bubble-induced reduction of species diffusivities. Hydrogen-caused OH^- transfer enhancement at the anode is favored for the cell performance improvement. According to our model, hydrogen effect on the current density mainly comes from two aspects: i) mass transfer alteration and ii) effective conductivity reduction. At either high or low velocity, parasitic hydrogen formation decreases the cell current densities, indicating that the conductivity reduction plays a predominant role. Through a preliminary evaluation of hydrogen contribution to the power output, we found that in a wide range of cell voltages, the utilization efficiency of anode material with parasitic corrosion is comparable to that of anode without corrosion assuming hydrogen utilization efficiency reaches 100%.

ACKNOWLEDGMENT. The authors would like to acknowledge the support from the CRCG and UDF of the University of Hong Kong.

REFERENCES

(1) Yang, S. H.; Knickle, H. *J. Power Sources* **2002**, *112*, 162-173.

(2) Ferrando, W. A. *J. Power Sources* **2004**, *130*, 309-314.

(3) Doche, M. L.; Novel-Cattin, F.; Durand, R.; Rameau, J. J. *J. Power Sources* **1997**, *65*, 197-205.

(4) Zhuk, A. Z.; Sheindlin, A. E.; Kleymenov, B. V. *J. Power Sources* **2006**, *157*, 921-926.

(5) Carbonio, D. J.; Tryk, D.; Yeager, E. *The Electrochemical Society Softbound Proceedings Series*, Pennington, NJ, **1987**.

(6) Yang, S. H.; Knickle, H. *J. Power Sources* **2003**, *124*, 572–585.

(7) Newman, J.; Thomas-Alyea, K. E. *Electrochemical Systems*, Third edition, A john wiley&sons, Inc., NJ, **2004**.

(8) Shah, A. A.; Al-Fetlawi, H.; Walsh, F. C. *Electrochim. Acta* **2010,** *55*, 1125-1139.

(9) Gu, W. B.; Wang, C. Y. *J. Electrochem. Soc.* **1997**, *144*(6), 2053-2061.

(10) Phillipe, M.; Jerome, H.; Sebastien, B.; Gerard, P. *Electrochim. Acta* **2005**, *51*, 1140-1156.

(11) Chan, K. Y.; Savinell, R. F. *J. Electrochem. Soc.* **1991**, *138*(7), 1976-1984.

(12) Yang, S. H.; Yang, W. Q.; Sun, G. Q.; Knickle, H. *J. Power Sources* **2006**, *161*, 1412–1419.

(13) Manninen, M.; Taivassalo, V. *On the Mixture Model for Multiphase Flow*, Valtion Teknillinen Tutkimuskeskus, **Finland**, **1996**.

(14) Wang, C. Y. *Chem. Rev.* **2004**, *104*, 4727-4766.

(15) Bruggeman, D. A. G. *Ann. Phys.* **1935**, *24*, 659.

Table I Properties and kinetics used in numerical simulations.

	Parameters
Geometrical parameters	Cell 1(AT400)[a]: L = 13cm, S = 0.14cm; Cell 2: L = 4cm, S = 0.2cm.
Physical properties of Substance	$D_{OH^-,0} = 5.26\times10^{-9} m^2/s$ [a], $D_{Al(OH)_4^-,0} = 10^{-9} m^2/s$ [a], $\rho_l = 1150 kg/m^3$ [a], $\mu_l = 0.0008 kg/(m\cdot s)$ [a], $\rho_g = 0.08189 kg/m^3$ [b], $\mu_g = 8.411\times10^{-6} kg/(m\cdot s)$ [b], $d_g = 2.6\times10^{-5} m$ [c], $\kappa_0 = 80 S/m$ [a]
Anode kinetics	
Main	$J_{m0} = 137.1 A/m^2$ [a], $\alpha_m = 007956$ [a], $\beta_m = 0.9204$ [a], $\gamma_m = 0.5$ [a], $\lambda_m = 1$ [a], $n_m = 1$ [a], $E_m^{eq} = -2.4403V$ [a]
Parasitic	$J_{p0} = 111.9 A/m^2$ [a], $\beta_p = 0.0591$ [a], $n_p = 1$ [a], $E_p^{eq} = -0.9058V$ [a]
Cathode kinetics	$k = -3.898\times10^4 A/(m^2\cdot V)$ [d], $b = -1.3904\times10^4 A/m^2$ [d], $E_c^{eq} = 0.2857V$ [a]
Operating conditions	$T = 333K$, $C_{OH^-}^{ref} = 5000 mol/m^3$, $C_{Al(OH)_4^-}^{ref} = 500 mol/m^3$
Constants	$F = 96500 C/eq.$, $R = 8.314 J/(mol\cdot K)$, $g = 9.81 m/s^2$

[a] from (11)

[b] from FLUENT database

[c] from (6)

[d] from (12)

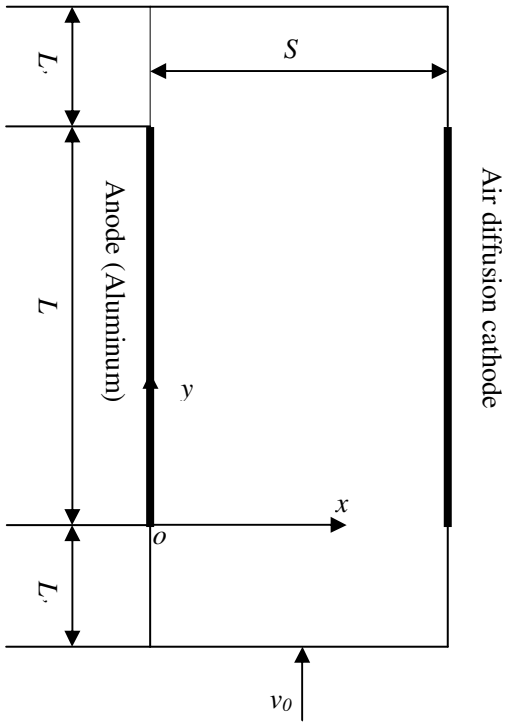

Figure 1. Schematic of the aluminum-air cell.

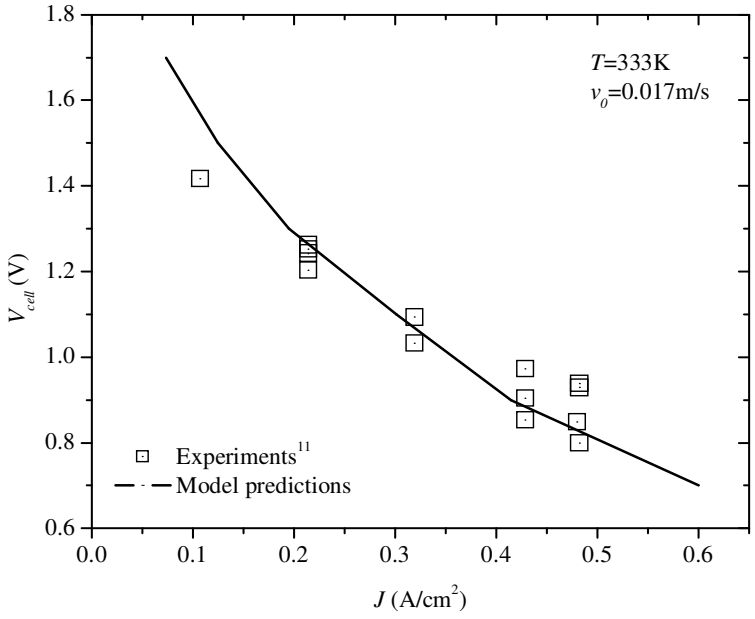

Figure 2. AT400 performance compared with the model predictions.

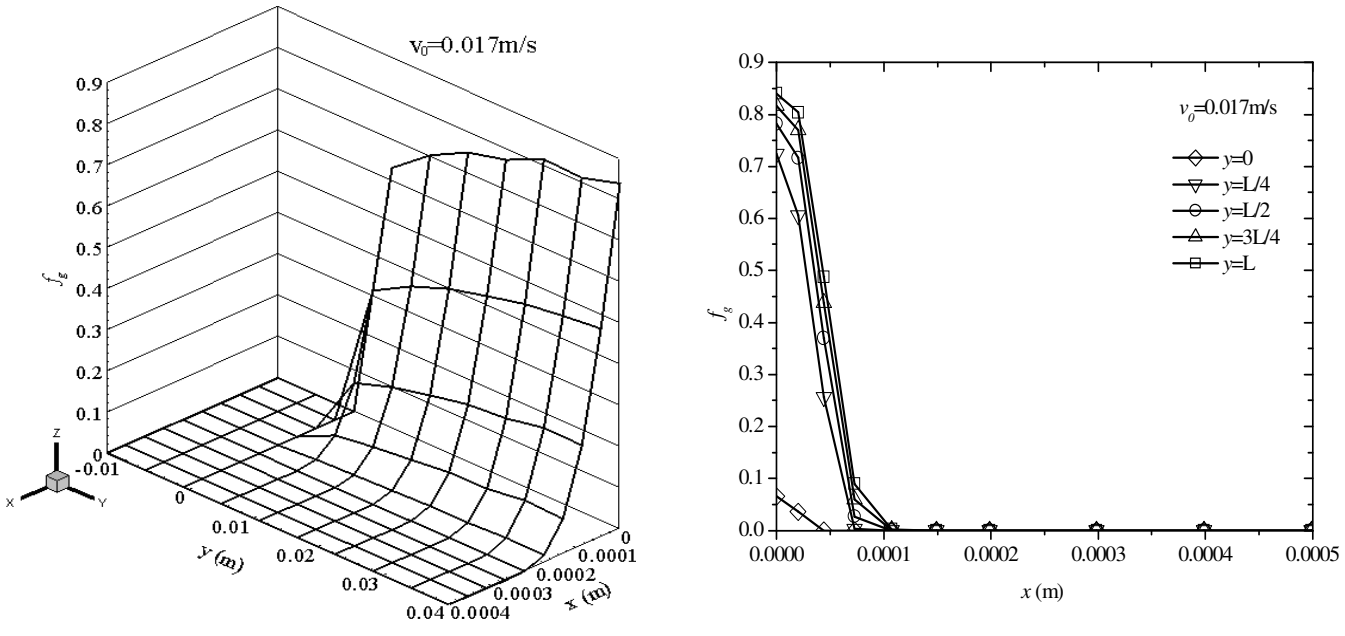

(a) (b)

Figure 3. (a) Hydrogen volume fraction distribution inside the cell and entrance regions. (b) Lateral distributions of hydrogen at different *y* positions.

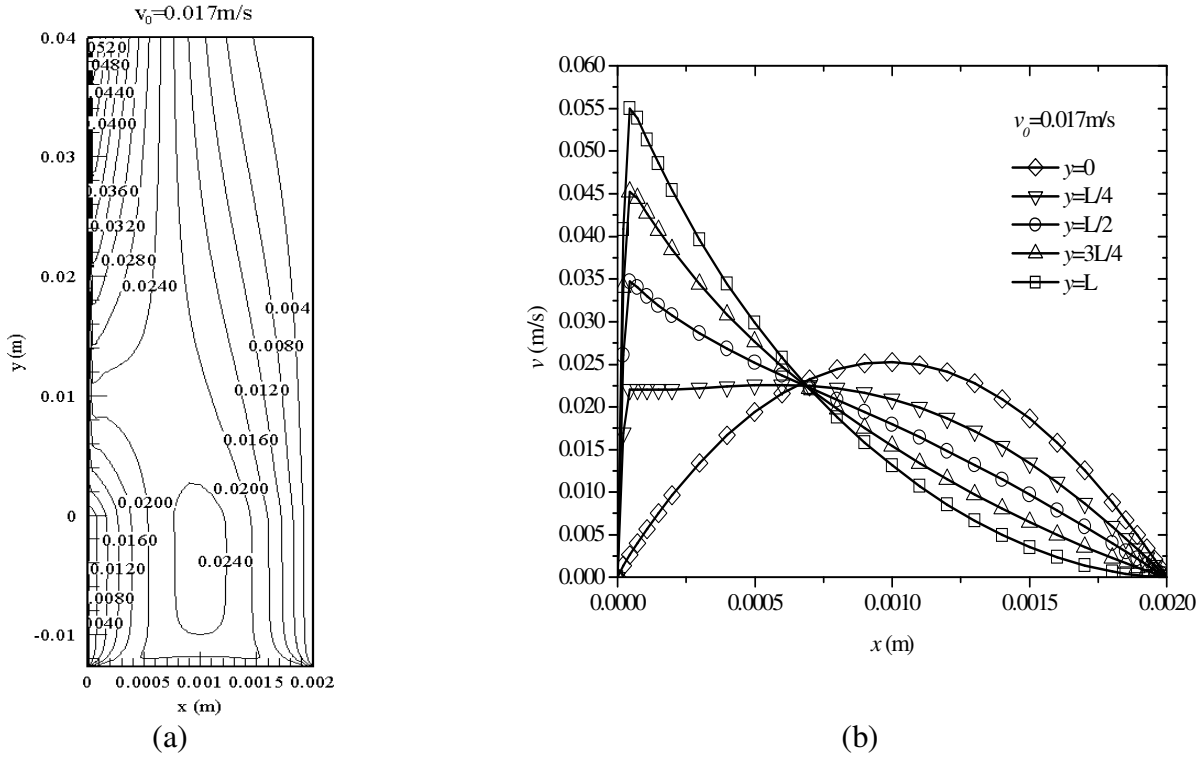

(a) (b)

Figure 4. (a) Velocity distribution inside the cell region. (b) Lateral distributions of velocity at different *y* positions.

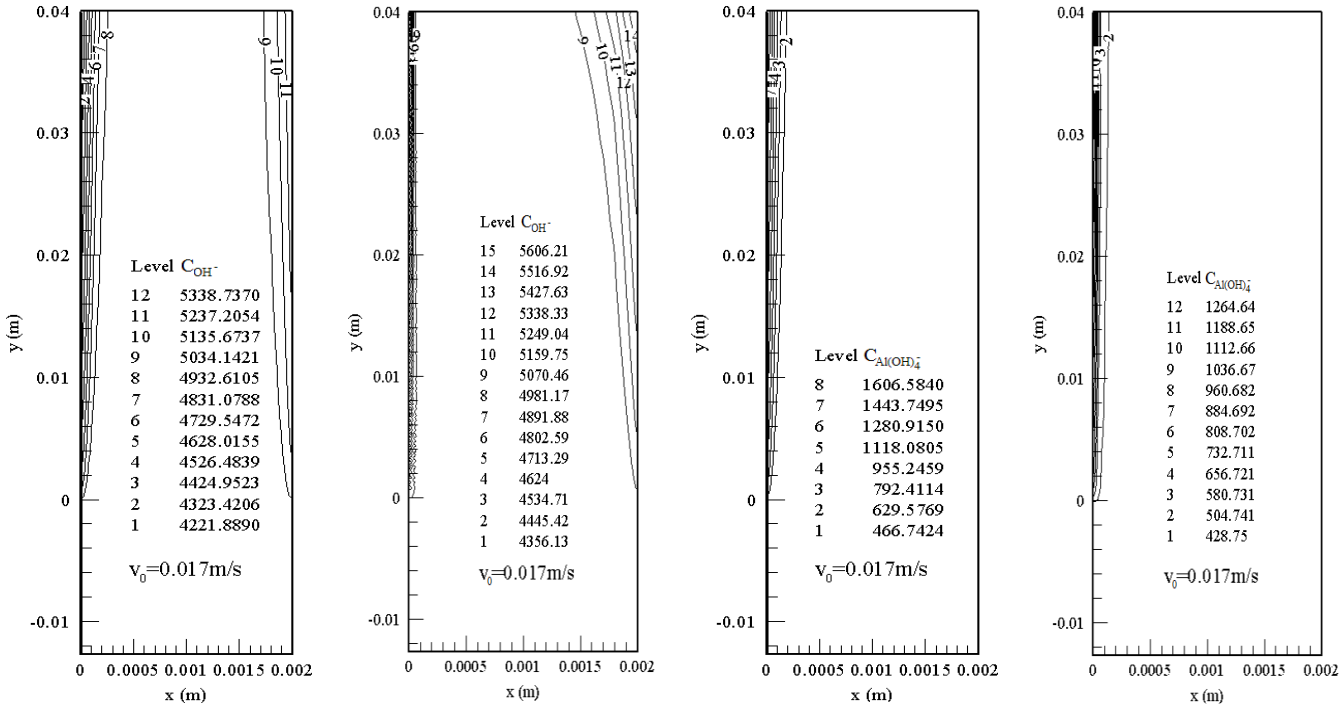

Figure 5. (a) OH^- distribution without hydrogen evolution. (b) OH^- distribution with hydrogen evolution. (c) $Al(OH)_4^-$ distribution without hydrogen evolution. (d) $Al(OH)_4^-$ distribution with hydrogen evolution.

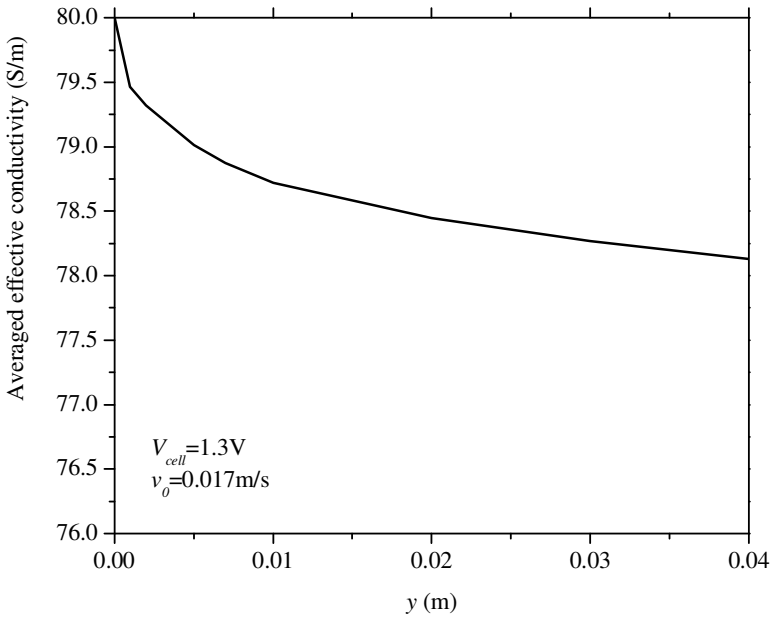

Figure 6. Averaged conductivity variation along the cell.

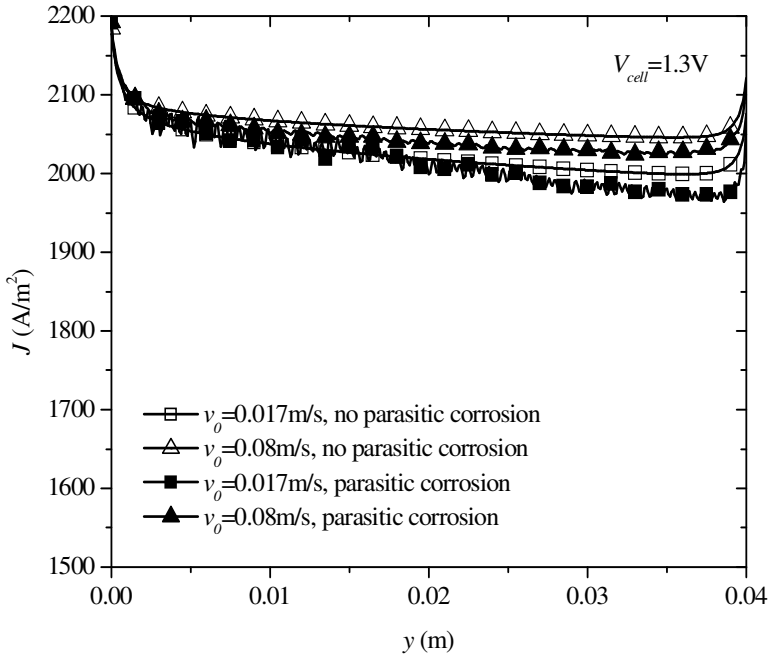

Figure 7. Effect of parasitic corrosion on current density distribution along the electrode.

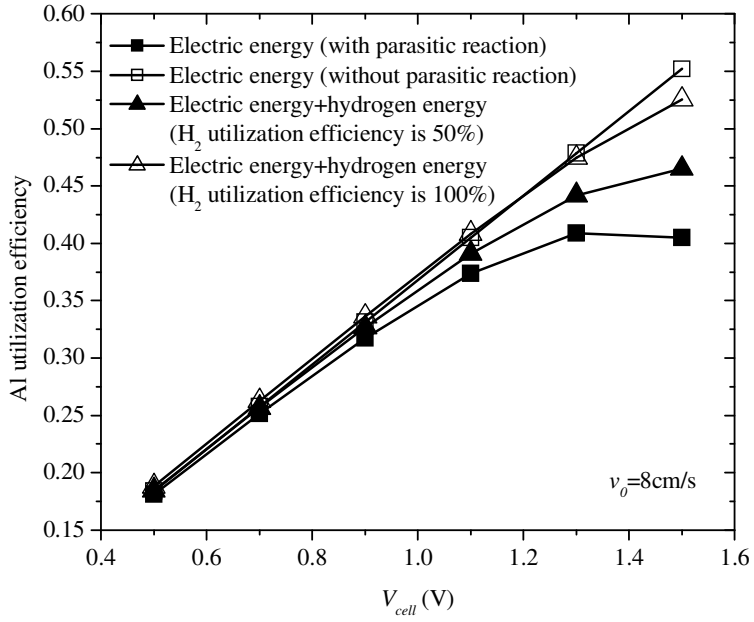

Figure 8. Aluminum utilization efficiency comparisons under different conditions